



Evaluating the sonic layer depth relative to the mixed layer depth

Robert W. Helber,¹ Charlie N. Barron,¹ Michael R. Carnes,¹ and Robert A. Zingarelli¹

Received 18 October 2007; revised 4 January 2008; accepted 28 February 2008; published 24 July 2008.

[1] Using a global set of in situ temperature and salinity profile observations, the sonic layer depth (SLD) and the mixed layer depth (MLD) are analyzed and compared over the annual cycle. The SLD characterizes the potential of the upper ocean to trap acoustic energy in a surface duct while MLD characterizes upper ocean mixing. The SLD is computed from temperature and salinity profile pairs using a new tunable method while MLD is computed using recently developed methods and either temperature only profiles or temperature and salinity profile pairs. Both SLD and MLD estimates provide information on different and important aspects of the upper ocean. The SLD and MLD often coincide because sound speed increases with depth down to the MLD, where (typically) a decrease in temperature occurs, resulting in a local maximum sound speed. The depth of this maximum sound speed is the SLD. The SLD and MLD are not always the same because sound speed is substantially more sensitive to temperature than to salinity compared to density. Since MLD is a commonly known and studied parameter, MLD is often used as a proxy for SLD in scientific and operational applications. In the boreal spring when fresh restratification events occur, the SLD is 10 m deeper (shallower) than the MLD in 39% (7%) of the observed profiles. A parabolic equation acoustic transmission model is used to evaluate the relative skill of the SLD and MLD estimates to predict surface acoustic trapping as measured by a simple metric.

Citation: Helber, R. W., C. N. Barron, M. R. Carnes, and R. A. Zingarelli (2008), Evaluating the sonic layer depth relative to the mixed layer depth, *J. Geophys. Res.*, 113, C07033, doi:10.1029/2007JC004595.

1. Introduction

[2] To further our understanding of the upper ocean's structure, we consider two parameters computed from vertical profile observations of temperature and salinity. The first is a commonly known parameter, the surface mixed layer depth (MLD), and a second parameter is the surface sonic layer depth (SLD). Each parameter provides a different characterization of the upper ocean.

[3] The MLD is the thickness of a surface layer that has nearly constant temperature, salinity, and density. Uniformity in the layer is due to turbulent mixing driven by momentum and buoyancy surface fluxes and shear at the base of the layer [Garrett, 1996]. The global variability of MLD is important to a wide variety of phenomenon from tropical cyclone formation [e.g., Mao *et al.*, 2000], to phytoplankton bloom critical depth theory [e.g., Siegel *et al.*, 2002], to climate variability [e.g., Deser *et al.*, 2003]. Numerical prediction of MLD is challenging in that the vertical structure of the temperature and salinity model fields tend to be overly smooth resulting in a shallow bias [Kara and Hurlburt, 2006].

[4] The SLD, in contrast, is the vertical distance from the ocean surface to the depth of a sound speed maximum. The

maximum in sound speed occurs at depth because in a layer where temperature and salinity are constant, sound speed increases with pressure until (typically) temperature, and therefore sound speed, decreases. The depth where sound speed is a maximum is the SLD. Often the SLD and the MLD coincide, because the sound speed is locally maximum at the base of the isothermal and/or isohaline surface layer. Figure 1 shows a typical example. As will be shown below, SLD and MLD are not always the same due to differences in the sensitivities of sound speed and density to temperature, salinity, and pressure. In general, sound speed is substantially more sensitive to temperature than to salinity compared to density.

[5] The SLD is of interest because it characterizes surface acoustic ducts. Depending on the SLD, there exists a Minimum acoustic Cutoff Frequency (MCF) above which sound tends to be "trapped" near the surface [e.g., Weston and Rowlands, 1979; Buckingham, 1991; Kerman, 1993; Etter, 2003]. Sound frequency (f) is the determining factor because frequency is inversely proportional to wavelength (λ) as governed by the relation $f = c/\lambda$, where c is the sound speed. If λ is long relative to the SLD, then $f < MCF$ and the sound is not "trapped" in an acoustic duct and is attenuated by spherical spreading, where intensity decreases as the inverse square of the range. If λ is short relative to the SLD, then $f > MCF$ and the sound is "trapped" in a surface acoustic duct and is attenuated by cylindrical spreading, where intensity decreases as the inverse of the range. Sound "trapped" in a duct can be transmitted for great distances.

¹Naval Research Laboratory, Stennis Space Center, Bay St. Louis, Mississippi, USA.

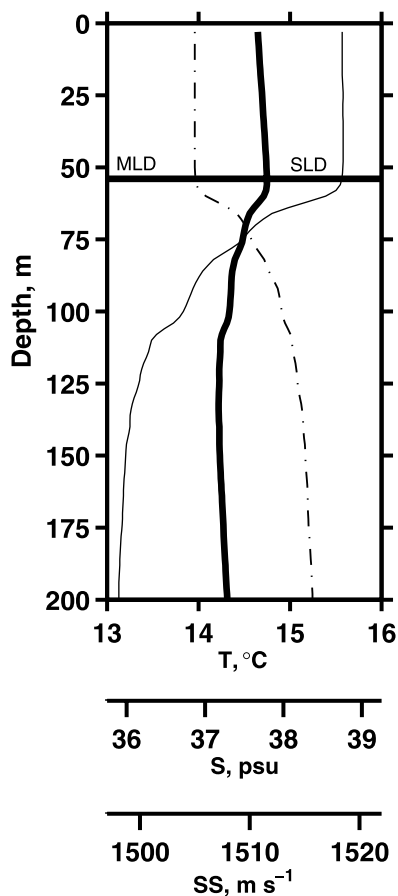


Figure 1. A typical profile pair of observed temperature (thin) and salinity (dash-dot) with computed sound speed (thick) versus depth. SLD and MLD coincide.

Hereafter, discussions regarding acoustic “trapping” are within this context. The MCF is dependent on the SLD, and the estimation method is described in section 3.2. Other factors such as bubbles and surface scattering influence the attenuation of acoustic energy, but spreading is the largest factor in the formation of surface acoustic ducts. Thus SLD and the associated MCF are the key characteristics of the upper ocean’s acoustic environment.

[6] The SLD variability is important for understanding the acoustic properties of the upper ocean that influence acoustic communications [e.g., *Siderius et al.*, 2007], acoustic tomography [e.g., *Sutton et al.*, 1993], and Navy operations related to hiding and detecting marine underwater vessels [e.g., *Urlick*, 1983]. Historically, scientific literature related to the SLD has been about surface acoustic ducts using a sound speed profile that is either measured [e.g., *Eden and Nicol*, 1973] or has an assumed functional form [e.g., *Bucker*, 1980]. A few studies address the upper ocean environment’s impact on the acoustics [e.g., *Sutton et al.*, 1993; *Lu et al.*, 2006]. *Siderius et al.* [2007] show that acoustic communications are strongly influenced by the diurnal cycle of the thermocline (or equivalently MLD). No studies relate the vertical sound speed structure with the vertical temperature or salinity structure observed in the ocean. It is a goal of this paper to examine this relationship and highlight how, when, and where differences between

SLD and MLD may occur over the global ocean on the annual cycle.

[7] In this analysis we rely on observed profiles of temperature and salinity with depth as measured by Conductivity-Temperature-Depth (CTD) recorders from a variety of platforms throughout the global ocean. Each profile describes the upper ocean at one location for approximately one instant in time, conditions produced by both past and present mixing. From this information, both SLD and MLD are estimated. The diurnal, seasonal, and interannual (decadal, etc.) variability have different influences on our interpretation and application of the MLD and SLD estimates.

[8] The highest resolution CTD profiles commonly available sample every 1 m and therefore do not measure the microstructure of the upper ocean. For this reason, in CTD profiles it has historically been difficult to distinguish between the penetration depth of present active mixing and the remnant MLD that results from mixing in the recent past [*Brainerd and Gregg*, 1995]. In this paper we refer to the depth of present active mixing penetration as the diurnal MLD and the remnant mixing penetration depth as the seasonal MLD. The reason for this distinction is that MLD estimated from observed CTD profiles is typically used to represent the seasonal MLD and this has been investigated by many authors [e.g., *Monterey and deWitt*, 2000; *Thomson and Fine*, 2003; *de Boyer Montégut et al.*, 2004]. Recently, *Lorbacher et al.* [2006, hereafter LDNK06] developed an algorithm that estimates the penetration depth of the most recent mixing events (the diurnal MLD) from observed temperature profiles. The LDNK06 algorithm is similar to earlier MLD methods by *Bathen* [1972] and *Belkin and Flyushkin* [1986] that search for the shallowest curvature peak for temperature and density profiles. These methods use the variance within the profile and do not depend on parameters that may change regionally or with time. In this analysis we use the LDNK06 methodology and their provided software for computing MLD that will be denoted MLD_{∇}^{∇} . The unadorned “MLD” will refer to the mixed layer depth in general or as otherwise noted. The superscript denotes that the methodology is based on profile curvature (or gradient ∇) while the subscript indicates only temperature profiles are required for its computation. The method can be applied to density profiles but the temperature only analysis is widely applicable because temperature profiles are globally far more numerous than profile pairs of temperature and salinity.

[9] The diurnal cycle may not be represented correctly in large-scale ocean numerical models. In these cases, the most recent mixing events selected from a profile by the LDNK06 algorithm may not correspond to the modeled MLD. An isopycnal threshold MLD algorithm for use with ocean general circulation models (OGCMs) was developed by *Kara et al.* [2000, hereafter KRH00] where the threshold sigma-t deviation ($\Delta\sigma_t$) is calculated for each profile. The $\Delta\sigma_t$ is computed using constant pressure, the profile’s salinity at 10 m, and a 0.8°C temperature change (ΔT). The MLD for this methodology is the depth where the density increases by $\Delta\sigma_t$ from its value at 10 m and will be denoted as MLD_{TS}^{Δ} , where the superscript, Δ , indicates that it is a threshold method and the subscript indicates that both

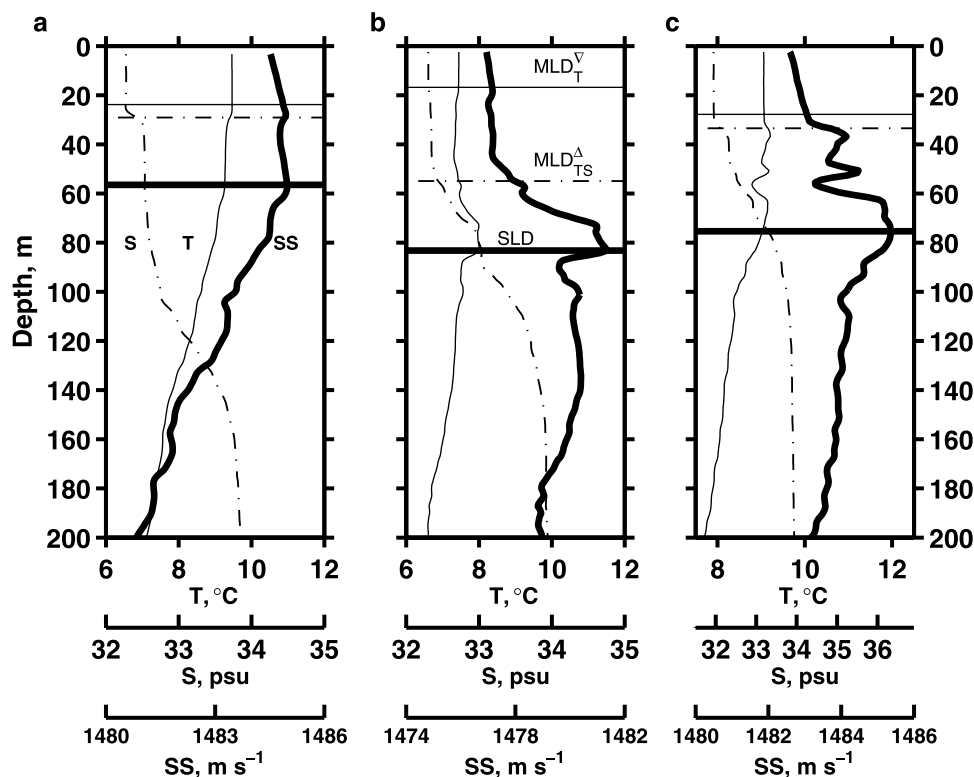


Figure 2. Typical temperature (thin curves; °C) and salinity (dashed-dot curves; psu) versus depth (m) observations. Sound speeds (thick curves; m s^{-1}) are also shown. The thin horizontal line is MLD_T^{∇} , with MLD_{TS}^{Δ} in the dashed-dot line and the SLD in the thick line. Cases of (a) shallow stratification, (b) temperature inversion, and (c) salinity dominated described in the text result in $SLD > MLD$. All three profiles have stable buoyancy.

temperature and salinity are required. These parameters are appropriate for observations with high or low vertical resolutions in all regions of the ocean, and the results tend not to capture the diurnal cycle (discussed in section 3.3). For this reason, we associate MLD_{TS}^{Δ} with the seasonal MLD. Kara *et al.* [2000] also used the 0.8°C threshold for a temperature based MLD estimate, but we have found that the σ_t threshold method matches more closely with SLD.

[10] Estimates of the surface acoustic ducts defined using climatologies or numerical model predictions are often inaccurate. Acoustics in the ocean are highly dependent on sound speed gradients, particularly where these gradients change sign. While climatologies and numerical model outputs may represent the mixed layer sufficiently for many purposes, the smoothed vertical gradients often found in these products may not adequately represent the actual acoustic properties of the upper ocean.

[11] Density responds differently than sound speed to depth gradients of temperature and salinity. These differences influence the SLD and MLD algorithms' selection of the layer depths. Each method searches for different types of changes in different parameters, often creating a bias between SLD and MLD. Estimating both SLD and MLD_T^{∇} from the data described in section 2 using methods described in section 3, we find that 39% of the ocean profiles have SLD and MLD_T^{∇} within 2 m of each other and 19% have a difference of at least 20 m. Typically, this bias is

manifested in profiles with small near-surface deviations in temperature and/or salinity that result in a shallow MLD_T^{∇} while the SLD remains deeper. An example of this is shown in Figure 2a. In this case, the increase of sound speed with pressure is greater than the decrease in sound speed associated with the small shallow temperature and salinity changes. This deep bias of SLD relative to MLD_T^{∇} typically occurs after events associated with spring and diurnal warming that stratify the upper ocean.

[12] Another typical example of profiles where SLD is greater than MLD has a temperature inversion that creates a deep sound speed maximum (Figure 2b). This profile has stable buoyancy since salinity increases through the temperature inversion. The third typical example is dominated by salinity resulting in a relatively shallow MLD and a deep SLD (Figure 2c). The small deviation in salinity at 33 m is enough to trip the density-based MLD_{TS}^{Δ} estimate, but for sound speed a larger salinity decrease is required to overcome increasing pressure, resulting in the SLD at 75 m.

[13] The examples in Figure 2 suggest that small anomalies in the vertical gradients of temperature and salinity profiles can have a large influence on the sound speed profile (and the acoustic properties of the upper ocean) and thereby create a large bias between MLD and SLD. The MLD identifies the depth penetration of turbulent mixing and is therefore dynamically linked to the upper ocean physics used in numerical prediction. In contrast, SLD is formed as a result of the temperature and salinity vertical

gradients that define the sound speed vertical gradients and is therefore indirectly linked to mixing processes. For these reasons, our ability to predict the MLD is more advanced than our ability to predict SLD. Understanding MLD/SLD differences will most importantly clarify the predictability of the acoustic properties of the upper ocean. Identifying the time and space extent of MLD/SLD biases will help characterize potential errors in numerical predictions of upper ocean acoustic properties used for communications, Navy operations, etc.

[14] The global CTD data set is described in section 2. For each CTD profile, the SLD and the associated MCF is estimated using methods described in section 3.2. The MLDs as defined by the LDNK06 and KRH00 (MLD_T^{∇} and MLD_{TS}^{Δ} , respectively) methods are also estimated for each profile. With this information we investigate the relationship of the acoustic trapping capability of the upper ocean to differences in SLD and the MLDs. An efficient metric is developed (section 3.1) to measure the trapping capability of the surface layer. The metric is optimized for speed and efficiency, instead of providing a definitive measure, because only the relative skill is required. For this end, a parabolic equation acoustic model is used to estimate the transmission range from a sound source at 10 m horizontally to an 80 dB loss. For comparison, a semi-empirical method to estimate acoustic trapping from SLD and both MLDs and their associated MCFs is also performed. The skill of each MLD is compared with the skill of the SLD for predicting trapping as determined by the acoustic model. This is done to evaluate potential errors when the prediction is based on (1) temperature only observations and (2) numerical model output that has skill for MLD_{TS}^{Δ} but may not represent the SLD correctly.

2. Data

[15] The goal of the data selection is identification of high quality temperature and salinity profiles that resolve both SLD and MLD while also providing a global distribution. An attempt has been made to remove potential errors and spikes due to noise by excluding profiles with extremely large vertical temperature and salinity gradients and profiles that are unstable.

[16] The CTD data from the World Ocean Database 2005 (WOD05) [Boyer *et al.*, 2006] and the U.S. Navy's Master Oceanographic Observational Data Set (MOODS) [Teague *et al.*, 1990] are combined. The depth profiles of temperature and salinity remain on the original observed depth sampling, and only those that do not have any substandard WOD05 or MOODS quality control flags are used. Since many data sources for the WOD05 and MOODS are the same, identical or nearly identical profiles exist in both data sets. These duplicates are identified as two or more profiles within 0.01° of latitude and longitude during the same hour. When duplicate WOD05 and MOODS profiles are found, the WOD05 profile is retained unless the MOODS profile has more depth levels. The addition of MOODS results in 6% more data than WOD05 alone. The total number of combined unique standard quality profiles with both temperature and salinity is 2,512,830.

[17] To ensure the data resolve the MLD and SLD, a profile is excluded if the shallowest depth sample is greater

than 10 m, the total depth range is less than 200 m, or the sampling interval is larger than 15 m. All depth levels with either temperature or salinity flagged as bad are also removed. Using these criteria reduces the number of profiles to 201,116. To remove noise, each profile is then smoothed using a three point normal distribution order statistic filter, often used for noise reduction in signal processing [Bovik *et al.*, 1983].

[18] The profiles with the 1% largest and smallest vertical gradients of temperature and salinity at any depth in the upper 200 m are also removed. Finally, the stability of each profile is defined as the first quartile of buoyancy frequency values computed versus depth. Profiles with stability below the lowest 10% of all profiles are excluded. Application of these restrictions further reduces the number of profiles to 190,330. Use of these strict requirements ensures that the surviving data sufficiently resolve the upper ocean while many data errors are likely removed.

3. Methods

[19] In this section we describe three approaches for characterizing the upper ocean. In section 3.1, we present a method for estimating the acoustic trapping capability of the upper ocean using a numerical acoustic model. In section 3.2, we explain how SLD and its associated MCF is estimated, while in section 3.3 we describe the characteristics of both MLD_T^{∇} and MLD_{TS}^{Δ} . Each of these provides a different characterization of the upper ocean. The goal of the present analysis is to characterize the differences between SLD and the MLDs and to evaluate the relative skill of the SLD and the MLD estimates to predict the acoustic trapping capability of the upper ocean as determined by a numerical acoustic model.

3.1. Acoustic Transmission

[20] A parabolic equation Range dependent Acoustic Model (RAM) is used to simulate an experiment with a single frequency sound source and a string of receivers, both at 10m depth, over a range of 20 km. The parabolic equation model represents acoustic transmission, using a finite difference Padé series solution that is calculated by marching outward from the sound source [Collins, 1994]. The solution is reliable at angles of at least 80° from horizontal at the source depth. To simulate the string of receivers, the RAM transmission loss at 10 m is range averaged using a 1 km characteristic length scale.

[21] The RAM simulations are used to determine the acoustic transmission range (ATR), a measure defined as the distance where the sound intensity transmitted horizontally from the source drops by more than 80 dB in a horizontally isotropic ocean. We are only investigating the near-surface acoustic trapping for ranges shorter than typical convergence zones. Acoustic bottom bounce and convergence zones are intentionally avoided by simulating a flat absorbing bottom at 2000 m. We assume a flat, still sea surface and do not account for the effects of near-surface bubbles or waves. While other factors influence acoustic transmission, spreading geometry has the largest impact. If the surface isothermal layer is sufficient for acoustic trapping, then the spreading of acoustic energy is cylindrical, while otherwise the spreading is spherical. Etter [2003]

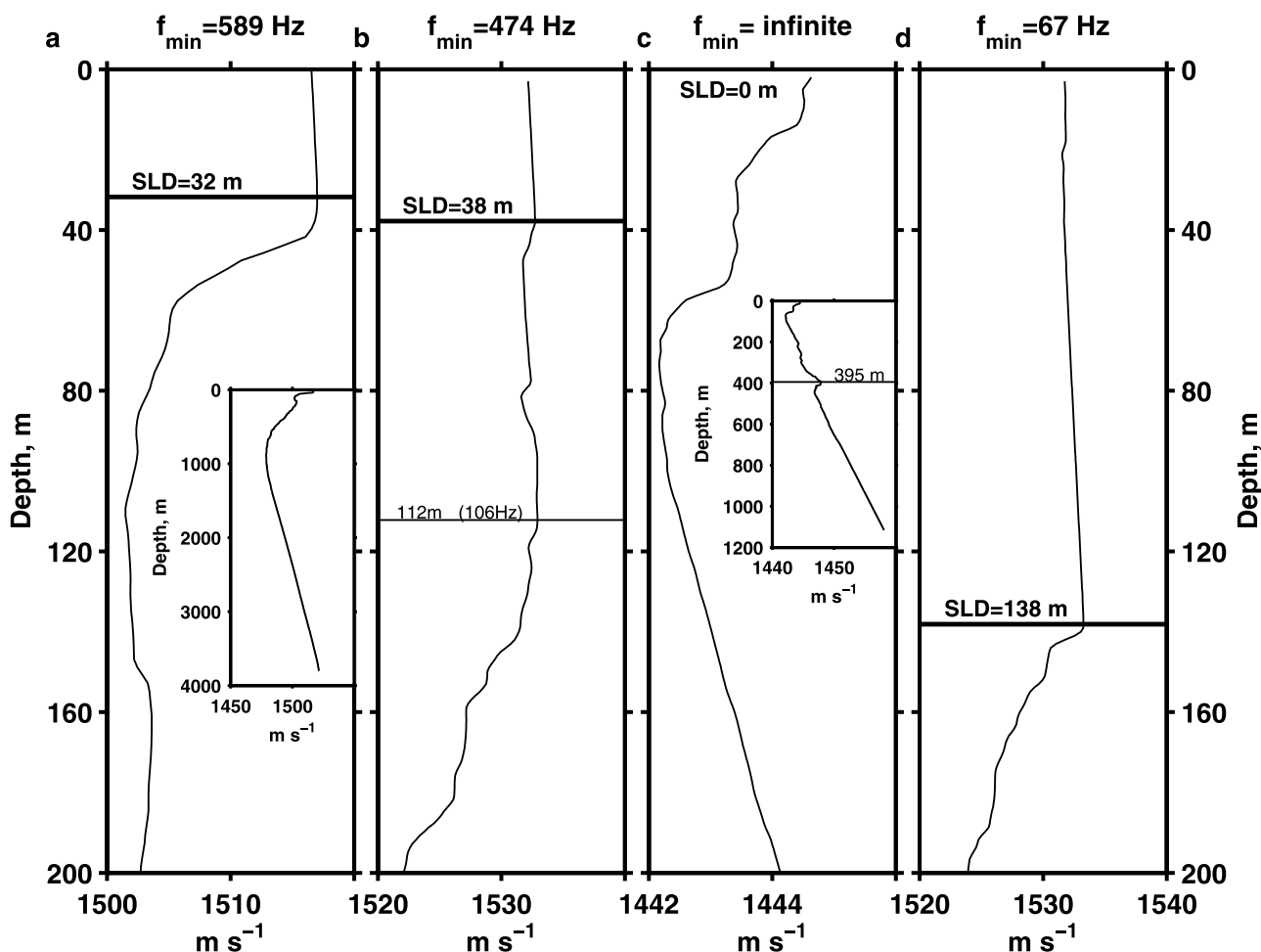


Figure 3. Sound speed profiles versus depth for (a) standard, (b) multiple surface duct, (c) absent surface duct, and (d) deep SLD cases. The MCF is labeled at the top of each panel, and the thick horizontal line in Figures 3a, 3b, and 3d represent the SLD as labeled. SLD in Figure 3c is zero. Figures 3a and 3c have inset figures that show the entire profile. The thin horizontal line in Figure 3b represents the base of a subsurface acoustic duct as labeled with depth and MCF in parentheses.

provides a complete discussion of acoustic transmission properties in the surface duct.

3.2. Sonic Layer Depth

[22] Sound speed is computed from profiles of temperature and salinity versus depth using the equation by Mackenzie [1981]. From the surface downward, a search is conducted for the depth of a sound speed local maximum, because in a surface duct the sound speed increases with depth toward a subsurface maximum, resulting in an upward refracting sound speed gradient. The search is for the depth of a sound speed local maximum that is larger than any shallower value and larger than the next deeper value. The search is not necessarily for the shallowest or deepest sound speed local maximum, but for a maximum sufficiently localized near the surface to trap relevant frequencies. Often there are larger sound speed values that occur much deeper below a deep sound channel, which do not represent SLDs. The algorithm described in this section, finds the relevant SLD without (in most cases) needing to search for a deep sound channel (special cases are discussed below). Since frequency is an important factor determining acoustic trap-

ping, two parameters that represent the lowest and mean acoustic frequencies (f_0 and f_{mean} , respectively) are used for tuning the SLD selection.

[23] For the present analysis, a set of five frequencies are chosen to span the low to midfrequency ranges uniformly in log space such that

$$f = \exp[\ln(70) + (\ln(2500) - \ln(70))r],$$

where r is a vector of five values: 0, 0.25, 0.5, 0.75, and 1. The resulting frequencies are 70, 171, 418, 1023, and 2500 Hz, and the mean of a uniform log space distributed set of frequency in this range is 680 Hz. Based on these frequencies the tuning parameters are $f_0 = 70$ Hz and $f_{mean} = 680$ Hz.

[24] Many profiles have more than one near surface local maximum sound speed value. In these cases a hierarchy of surface ducts exist, each capable of trapping an increasingly lower frequency of sound in an increasingly large depth range. An example in Figure 3b is discussed below. The goals of the selection criteria are to find the most relevant duct for the application and to avoid choosing deep sound

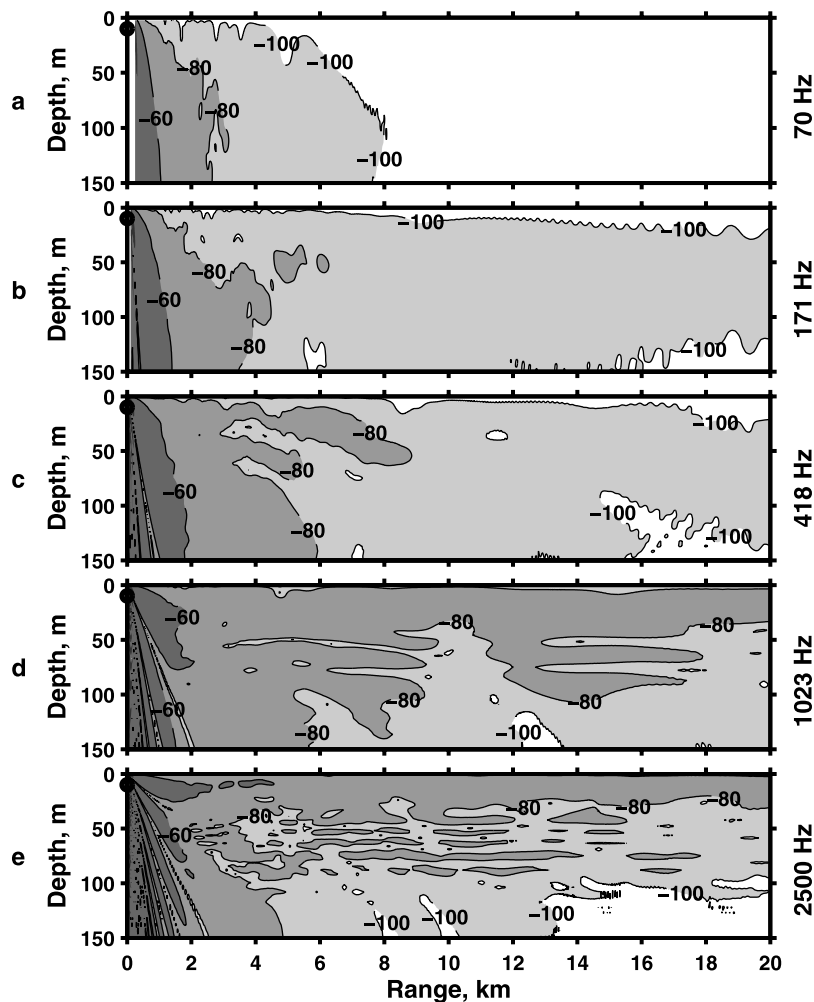


Figure 4. Range versus depth acoustic transmission loss computed using the RAM in range independent mode at frequencies (a) 70, (b) 171, (c) 418, (d) 1023, and (e) 2500 Hz for a source at 10 m (dark circle) and the profile shown in Figure 2b. The dB acoustic transmission loss is relative to the loss at a range of 1 m. Contours are drawn at: -40 , -60 , -80 , and -100 dB.

speed values that may occur below the deep sound channel. To do this, determining the MCF is a necessary calculation.

[25] Using a method originally derived for atmospheric trapping of short radio waves [Kerr, 1951], the MCF is given by [see also Etter, 2003]

$$MCF = \bar{c} \left\{ \frac{3}{8} \sqrt{2} \int_0^{SLD} \left[\frac{c(SLD)}{c(z)} - 1 \right]^{1/2} dz \right\}^{-1} \quad (1)$$

where z is the vertical coordinate that is zero at the ocean surface and positive downward, \bar{c} is the average sound speed over the depth range from zero to SLD, and $c(z)$ is the sound speed at depth z . Equation (1) is calculated directly from a discrete sound speed profile using the trapezoid integration method. Equation (1) is also valid for a subsurface duct if the limits of integration are set to the upper and lower depths of the duct.

[26] While typical profiles often have one surface duct above a deep sound channel (Figure 3a), many profiles support more than one potential surface duct (Figure 3b). In these cases, we need to identify among multiple options the

SLD that will trap nearest the surface the largest range of expected frequencies. The duct selected is the shallowest that will trap a frequency less than f_{mean} . The 38 m duct was chosen for the SLD in Figure 3b instead of the 112 m duct because the 38 m duct has a MCF of 474 Hz that is less than f_{mean} . This indicates that the profile will trap most of the acoustic frequencies for this application (identified by f_0 and f_{mean}) above 38 m depth.

[27] The deeper duct extending to 112 m can trap 106 Hz but is not chosen because lower frequencies from a source at 10 m will spread broadly over 100 m rather than remaining within a concentrated duct near the surface. At frequencies of 171 and 418 Hz, the longest horizontal transmission ranges occur at deeper depths between 40 and 80 m (Figures 4b and 4c). This is technically a trapping environment for these frequencies, but the acoustic energy is not tightly trapped at the surface. Instead sound tends to focus near the subsurface minimum (the sound channel axis) located near 80 m (Figure 3b).

[28] For the profile in Figure 3b, a sound source at 10 m transmits acoustic energy with little or no surface trapping for frequencies 70, 171, and 418 Hz (Figures 4a, 4b, and 4c).

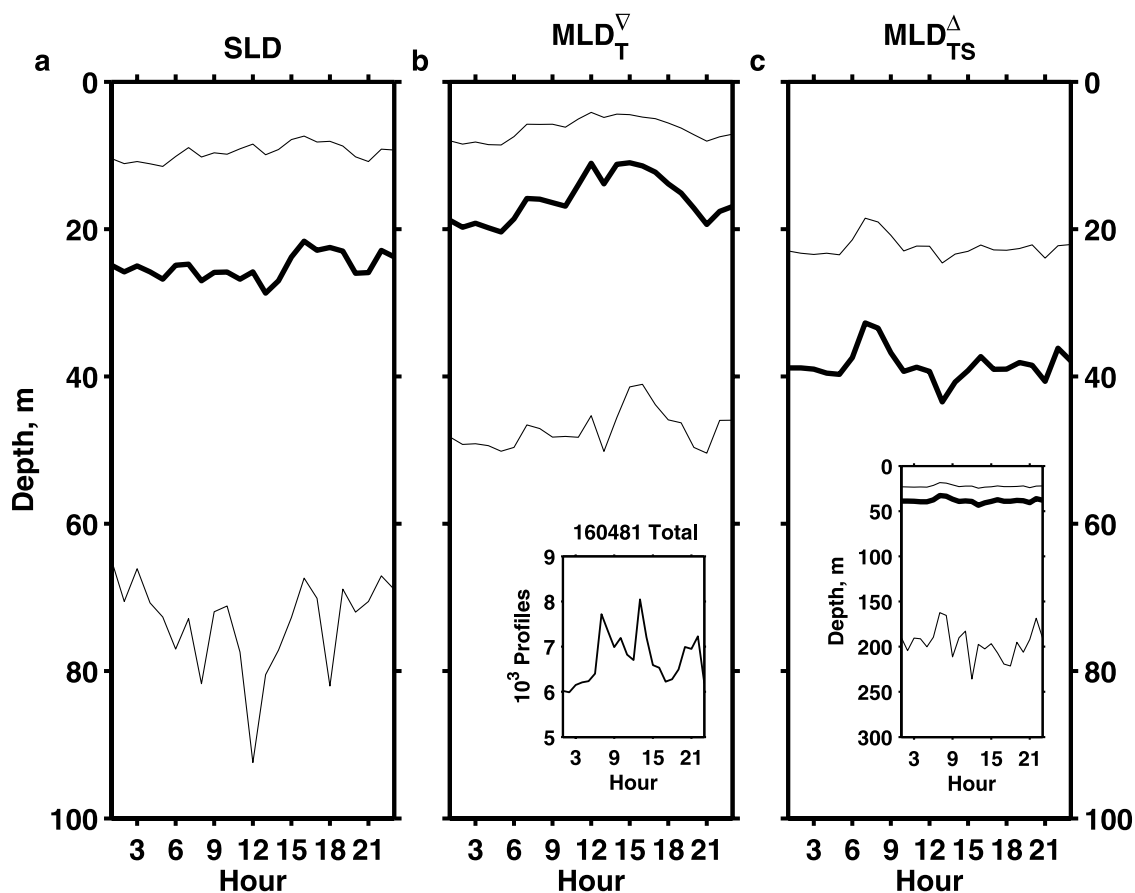


Figure 5. First quartile (upper thin lines), median (thick lines), and third quartile (lower thin lines) values for (a) SLD, (b) MLD_T^{∇} , and (c) MLD_{TS}^{Δ} versus the local time of day from the 160,481 profiles. The inset figure in Figure 5b shows the number of profiles versus local time. The inset figure in Figure 5c shows the 300 m depth range in order to include the third quartile for MLD_{TS}^{Δ} that resides between 150 and 250 m.

Acoustic transmission with a loss less than 80 dB does not extend in range farther than 10 km at all depths. As a result, the ATR is also less than 10 km for these frequencies. At frequencies higher than 474 Hz, the MCF for the profile in Figure 3b, there is acoustic trapping near the surface and the ATR is greater than 20 km (Figures 4d and 4e). For this reason the SLD at 38 m is the most relevant SLD for this profile and is chosen since it is the shallowest potential duct with a MCF less than f_{mean} . This is the method for selecting the SLD for every multiple duct profile.

[29] Another potential pitfall occurs where the first sound speed local maximum has a MCF lower than f_0 . In many cases, a low MCF is due to a very deep SLD as in Figure 3d. There are cases with a very low MCF that do not have a surface duct but have only a deep sound channel as in Figure 3c. In cases with only a deep sound channel and no surface duct, the SLD is set to zero. This is because acoustic energy will not be tightly focused near the surface. Instead sound will be refracted toward the sound channel axis (located at the depth of the sound speed minimum). The MLD is also zero in these cases.

[30] We distinguish between the case with a deep SLD (as in Figure 3d) and the case with only a deep sound channel (as in Figure 3c) by searching for a deep sound channel

above the sound speed local maximum. In the case of Figure 3c there is a sound speed local maximum at 395 m with a subsurface duct above that. If the subsurface duct can trap a frequency of f_{mean} or less (as in the case in Figure 3c), then the SLD is zero. Alternatively, if there is no subsurface duct above a deep sound speed local maximum, then the depth of the maximum is the SLD (Figure 3d). The algorithm searches for these cases whenever the first sound speed local maximum has a MCF lower than f_0 .

3.3. Mixed Layer Depth

[31] The methods for estimating the MLD from observed profiles are taken from LDNK06 and KRH00 (MLD_T^{∇} and MLD_{TS}^{Δ} , respectively). Software for both methods is freely available. These methods were chosen because they represent different characterization of the upper ocean by virtue of their methodology. The MLD_T^{∇} methodology uses the change in vertical gradients (i.e., curvature) to identify the MLD, while the MLD_{TS}^{Δ} methodology uses a threshold change in density from the 10 m profile value. The MLD_T^{∇} provides the depth of the isothermal layer that is associated with the diurnal cycle, while the MLD_{TS}^{Δ} more closely represents the seasonal MLD. The MLD_T^{∇} method only requires temperature profiles while MLD_{TS}^{Δ} requires both temperature and salinity profile pairs to compute σ_t .

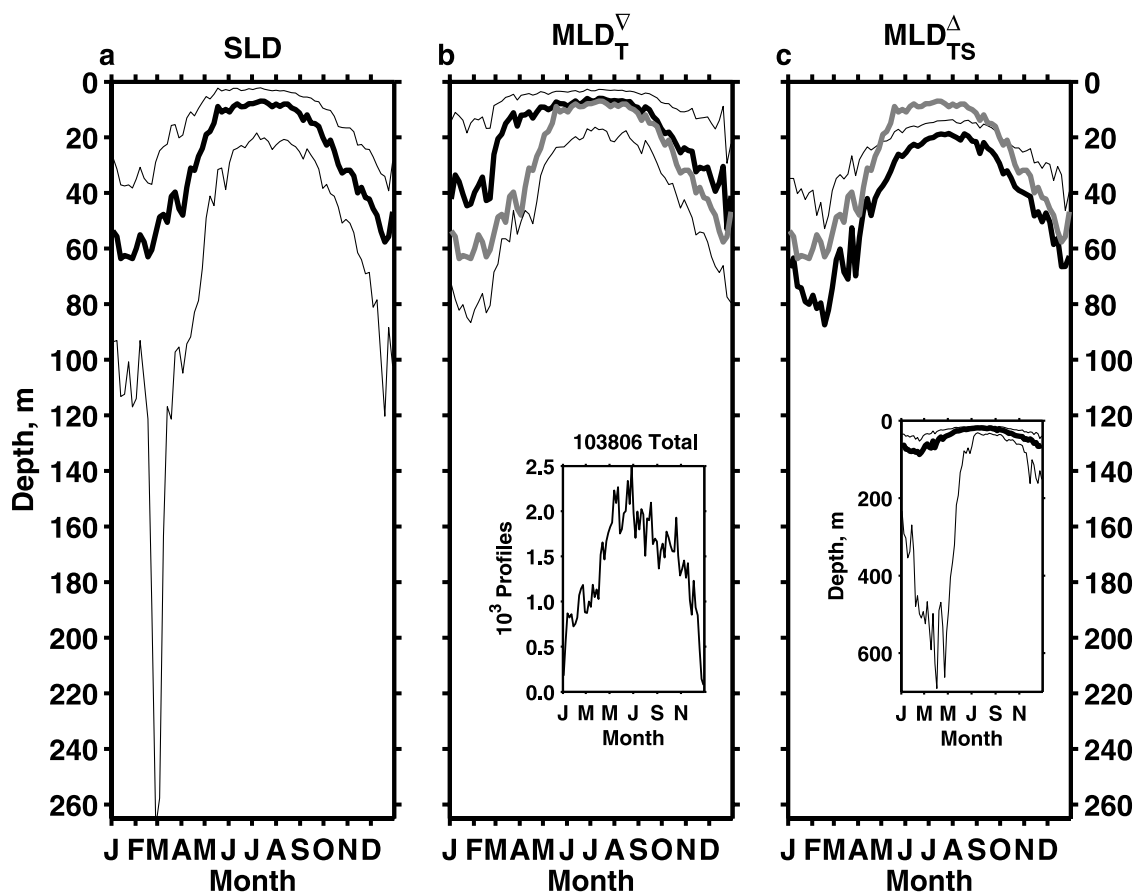


Figure 6. First quartile (upper thin lines), median (thick lines), and third quartile (lower thin lines) values for (a) SLD, (b) MLD_T^{∇} , and (c) MLD_{TS}^{Δ} versus day of year from 83,098 profiles north of 10°N and south of 60°N . For comparison, the SLD median line is repeated as a thick gray line in Figures 6b and 6c. The inset figure in Figure 6b shows the number of profiles versus day of year. The inset figure in Figure 6c shows the 700-m depth range in order to include the third quartile.

[32] Figure 5 shows the first, second (median), and third quartiles of SLD, MLD_T^{∇} , and MLD_{TS}^{Δ} versus local time of day, computed from the 160,481 profiles for which the time of day for the cast was available. The remaining profiles only identify time by month and year. The MLD_T^{∇} is shallow relative to SLD, has the smallest variance, and is the only algorithm that suggests a diurnal cycle (Figure 5b). The MLD_{TS}^{Δ} has the largest variance and a substantial deep bias relative to the SLD. Due to the large variance the diurnal cycle is not statistically significant. More detailed analysis in smaller coherent regions is needed to investigate the diurnal cycle and is outside the scope of this paper. An interesting but unrelated result is that fewer historical profiles exist during late-night and lunch and dinner time hours (inset plot of Figure 5b).

[33] While the diurnal cycle is present in the data, this article focuses on the annual cycle of SLD and MLD. Figure 6 shows the first, second (median), and third quartiles of SLD, MLD_T^{∇} , and MLD_{TS}^{Δ} versus year day, computed from the 103,806 profiles that have day values and are north of 10°N and south of 60°N . The statistics were computed from 5 day bins for all years of data. This latitude range is chosen to show the seasonal cycle in the data rich Northern

Hemisphere. The median is used to characterize the seasonal cycle because the histogram of SLD and MLD is shaped like a gamma distribution with a very long tail for deep depths. The histogram of the MLD_T^{∇} method does not have such a long tail for deep profiles. Very deep SLD and MLD_{TS}^{Δ} exist at high latitudes during winter months when the entire water column is well mixed. Taking an average over space and time where very deep values occur results in a mean that is skewed deeper. The median minimizes this effect.

[34] There is a lag in the shallowing of SLD relative to MLD_T^{∇} annually in February, March, and April. During these months MLD_T^{∇} tends to be shallower (Figure 6b) by approximately 20 m. While the MLD_{TS}^{Δ} has a deep bias relative to SLD throughout the year, this bias is slightly reduced in the spring (Figure 6c). Reducing the MLD_{TS}^{Δ} threshold ΔT value from 0.8 to 0.2°C reduces the deep bias relative to SLD for much of the year (Figure 7), and the variance (not shown) is reduced but still large relative to the SLD and MLD_T^{∇} variance. For May through September, MLD_{TS}^{Δ} remains deeper than SLD for all ΔT values from 0.8 to 0.2°C . This is consistent with the spring MLD (of any method) shallowing relative to SLD. The MLD_{TS}^{Δ} threshold ΔT value could be tuned to match the SLD in spring and

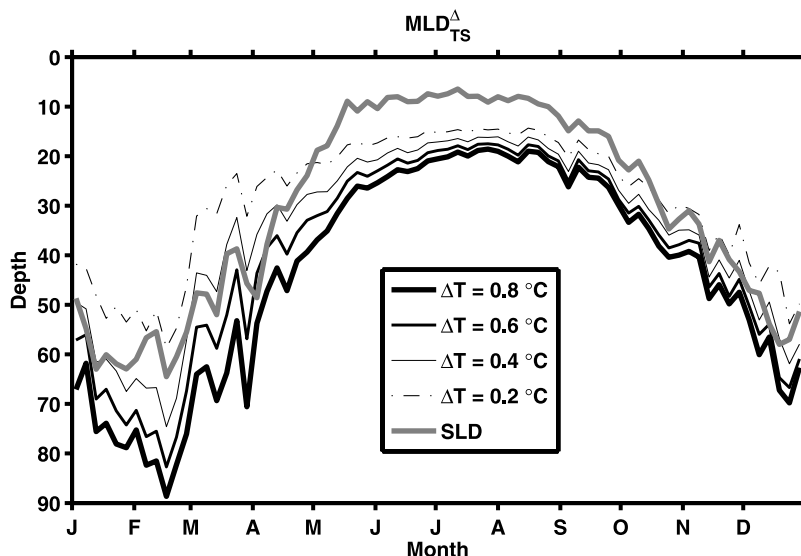


Figure 7. Median values for MLD_{TS}^{Δ} using a ΔT thresholds of 0.2, 0.4, 0.6, and 0.8°C (see legend) versus day of year from 83,098 profiles north of 10°N and south of 60°N. For comparison, the SLD median line is the thick gray line.

fall, but the variance is still large and the deep bias would remain during the summer.

4. Results

4.1. Mixed Versus Sonic Layer Depth

[35] To further highlight the seasonality of the differences between SLD and MLD_T^{∇} , we consider the median bias, correlation coefficient, and root mean square error. The results for MLD_{TS}^{Δ} are not shown because the seasonality is not pronounced. In Figure 8 the data are binned at ten day (of the year) and 20 degree (latitude) intervals. Median bias is computed as the median of SLD minus MLD_T for each bin (Figure 8a). Root mean square error (Figure 8b) is computed for each bin as

$$RMSE = \sqrt{\Sigma(SLD - MLD_T^{\nabla})^2}.$$

Correlation coefficient (Figure 8c) is computed for each bin as

$$r_{SLD,MLD_T^{\nabla}} = \frac{1}{N-1} \Sigma \left[(SLD - \overline{SLD}) \cdot (MLD_T^{\nabla} - \overline{MLD_T^{\nabla}}) \right] / S_{SLD} S_{MLD_T^{\nabla}},$$

where S_{SLD} , S_{MLD} , \overline{SLD} , and $\overline{MLD_T^{\nabla}}$ are the standard deviations and the mean values for SLD and MLD_T^{∇} respectively.

[36] Notice that median bias has strong seasonality for latitudes higher than 30°, both north and south. At very high latitudes, particularly near Antarctica, penetrative convection produces a relatively well-mixed water column where sound speed mainly increases with pressure. The sound speed maximum is usually at the bottom, making the SLD much deeper than the MLD_T^{∇} . SLD has large deep biases in northern hemisphere spring and southern hemisphere

summer and fall. SLD is slightly deeper than the MLD_T^{∇} throughout the year in the tropics. Similar seasonality exists in the RMSE in the northern hemisphere, but the southern hemisphere tends to have large RMSE for most the year. Correlation coefficient is generally weaker poleward of 30° though slightly larger in the northern hemisphere north of 40°N in June, July, August, and September.

[37] In the boreal spring for latitudes greater than 30°N, new mixing events typically make the MLD_T^{∇} shallower relative to the SLD (Figure 8a). In the spring 39% of the profiles have the SLD 10 m greater than the MLD_T^{∇} (Table 1). In the fall this is greatly reduced with only 11% of the profiles having a SLD 10 m greater than the MLD_T^{∇} . In the fall, when deep mixing occurs, the SLD and the MLD differ by less than 10 m for 86% (51%) of the profiles using the (MLD_{TS}^{Δ}) estimate.

[38] Figure 9 shows the global distribution of the biases in maps for each season of $SLD - MLD_T^{\nabla}$ averaged in 2 by 2 degree bins. During February through April, the northern hemisphere has many profiles with deep biases in SLD. The largest biases tend to occur in and near the Gulf of Alaska, Nova Scotia, the Mediterranean Sea, and the North Atlantic. During the opposite time of the year, from August through October, the bias is greatly reduced in the Northern Hemisphere, but in the Southern Hemisphere (austral spring) the bias occurs within the Antarctic Circumpolar Current. There appears to be a year-round bias near the Weddell Sea, the Arctic, and near the southernmost tip of Greenland. Scattered around the global ocean during all seasons are green squares representing a relatively small bias for SLD greater than MLD_T^{∇} . These more isolated cases occur when diurnal warming in the afternoon stratifies the near surface layers, reducing the MLD_T^{∇} but having no effect on the SLD which remains at the seasonal MLD.

4.2. Acoustic Trapping

[39] The transmission loss was modeled using RAM at the five frequencies described in section 3.2 for 3600

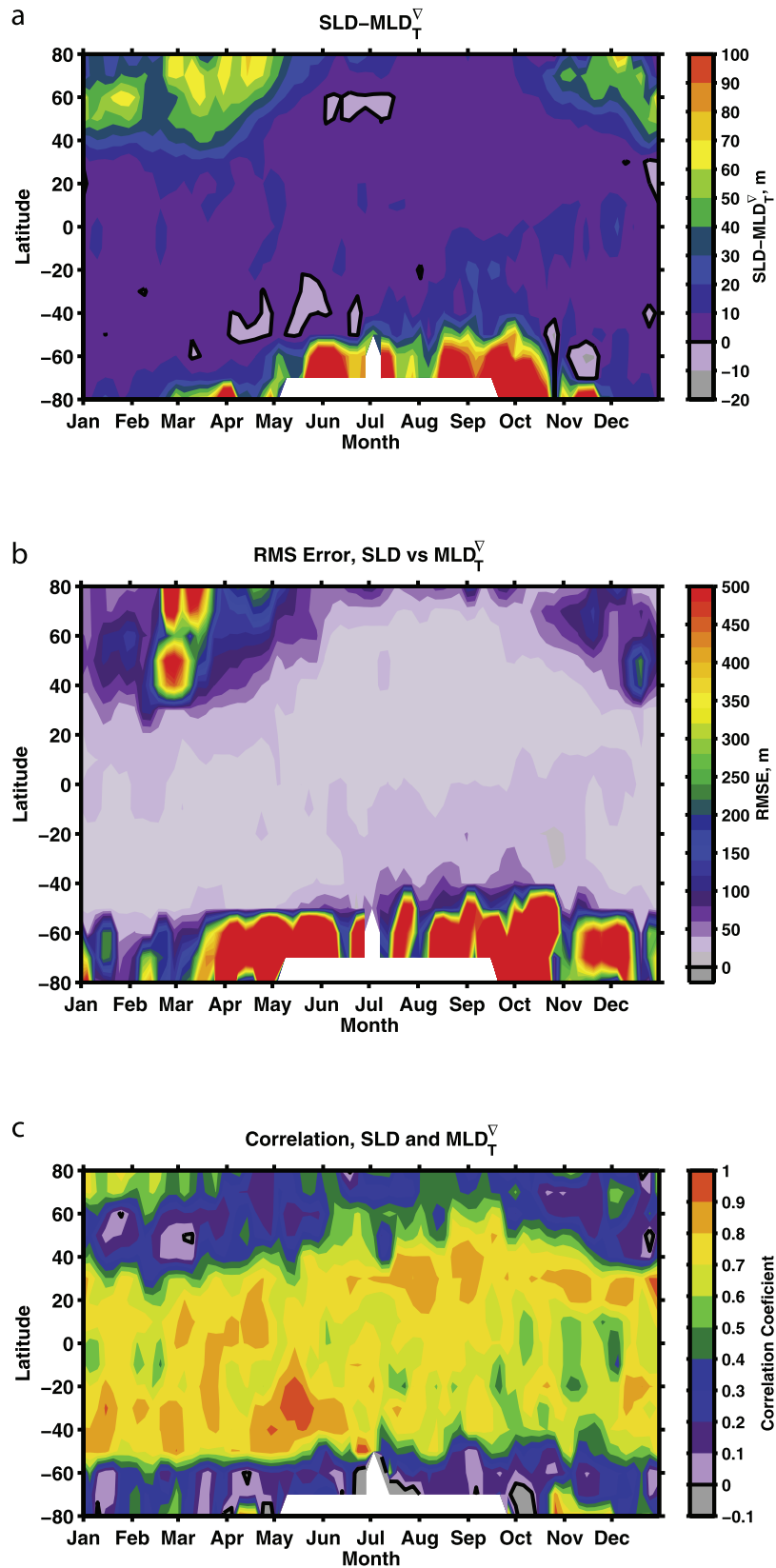


Figure 8. (a) The median bias for the annual cycle versus latitude computed from data binned over 10 days and 20 degrees of latitude. (b) The RMS error for the annual cycle versus latitude from data binned as in Figure 8a. (c) The correlation coefficient for the annual cycle versus latitude from data binned as in Figure 8a.

Table 1. Percentage of Profiles With SLD Deep, Negligible, and Shallow Bias Relative to MLD for Latitudes Between 10°N and 60°N

Season	MLD Method	$SLD > MLD + 10$	$ SLD - MLD < 10$	$SLD < MLD - 10$
Spring (FMA)	MLD_T^{∇}	39%	54%	7%
	MLD_{TS}^{Δ}	19%	18%	63%
Fall (ASO)	MLD_T^{∇}	11%	86%	3%
	MLD_{TS}^{Δ}	3%	51%	46%

randomly selected profiles north of 20°N. The input profiles are selected from north of 20°N in order to evaluate the boreal seasonal cycle, since it has been sampled more frequently than the southern hemisphere. The ATR is computed (as described in section 3.1) from the RAM output at 10 m that is range averaged with a characteristic length scale of 1 km. Thus an ATR value is obtained for all 3600 profiles at each frequency totaling 18000 values.

[40] A histogram of ATR from the 18000 RAM runs shows intermediate ranges where few profiles fall (Figure 10). The number of profiles with an ATR that is shorter than 5 km is 10,209 or 57%, while the number profiles with an ATR longer than 15 km is 6528 or 36%. Thus 92% of profiles have an ATR that occurs at the extremes. The intermediate ATR with the minimum number of occurrences is at 14 km. For this reason, ATR less than 14 km are considered a nontrapping environment, and ATR greater than 14 km are considered a trapping environment. Since the ATR from the RAM computations provide our best determination of whether trapping occurs at the source frequency, its values are taken as the “observed” or “reference” trapping/nontrapping results.

[41] To evaluate estimates of trapping/nontrapping using the SLD, we compare the associated MCF (equation (1)) with each of the five source frequencies. In this case, the SLD is estimated using f_{mean} equal to the source frequency. If the source frequency is greater than (less than) the MCF, we consider this to be a “prediction” for trapping (nontrapping). Thus each of the five “predictions” of trapping/nontrapping for each profile are compared with the corresponding “observed” RAM result.

[42] To evaluate predictions of trapping/nontrapping where SLD is not known or withheld, MLD_T^{∇} and MLD_{TS}^{Δ} are used in place of SLD. The MCF for these cases is determined using the value for each MLD instead of SLD. Ordinarily, equation (1) assumes that the integration is from the surface to the SLD. To ensure that sound speed increases with depth down to the MLDs we assume an isothermal and isohaline surface layer for the integration. Each of these five “predictions” of trapping/nontrapping for each profile and each MLD method are also compared with the corresponding “observed” RAM result.

[43] With these methods, we have a dichotomous verification situation that can be displayed in a 2×2 contingency table. The two results are trapping/nontrapping “observed” by the RAM versus trapping/nontrapping “predicted” by SLD/MCF. We have split up the numbers for each month to show the northern hemisphere seasonality (Figure 11). Since the range from a 10 m source to the 80 dB transmission loss is not a definitive estimate of acoustic trapping in the upper ocean, the SLD/MCF pairs have less than perfect skill with this metric (Figure 12). For this reason, we focus

on the relative skill of the MLDs and their associated MCF to predict trapping. For profiles north of 20°N, we find that the deep bias of the MLD_{TS}^{Δ} produces more true positives than the MLD_T^{∇} (Figure 11a). Conversely, the shallow bias of the MLD_T^{∇} produces more true negatives than even the SLD estimate (Figure 11d). Similarly, the MLD_{TS}^{Δ} has the most false positives while the MLD_T^{∇} has the most false negatives (Figures 11b and 11c). Of the two MLD methods, the overall skill for predicting trapping is greater for MLD_T^{∇} (Figure 12).

[44] Seasonality of SLD/MLD estimates is evident by the low (high) percentage of true positives (negative) in boreal summer (May, June, July, and August). During this season the MLD and SLD are relatively shallow. In boreal spring (March, April, and May) the MLD_T^{∇} has a larger percentage of false negatives associated with the spring warming events.

5. Summary and Conclusions

[45] The three parameters, SLD, MLD_T^{∇} , and MLD_{TS}^{Δ} each characterize the upper ocean in different ways. The SLD represents the potential of the upper ocean to trap acoustic energy in a duct near the surface. The SLD methodology requires profile pairs of temperature and salinity that are used to compute a sound speed profile. The MLD_T^{∇} is the penetration depth of the most recent surface mixing that is resolved in a profile as defined by potentially small changes in near surface vertical gradients of temperature. Salinity is not used for the MLD_T^{∇} . The MLD_{TS}^{Δ} is a density based threshold method that most closely represents the seasonal MLD and requires profile pairs of temperature and salinity. Vertical gradients of temperature and salinity are not considered directly in this methodology.

[46] Using a global set of in situ profile observations, we show that there exists a robust seasonal cycle in the differences between MLD_T^{∇} and SLD. The MLD_T^{∇} is shallower than SLD during spring when stratification events occur. In the northern hemisphere this occurs during February, March, and April in the Gulf of Alaska, Mediterranean Sea, New Foundland Basin, Labrador Sea, and far North Atlantic. During August, September, and October MLD_T^{∇} tends to be shallower than SLD in the southern hemisphere within the Antarctic Circumpolar Current. At high latitudes, SLD and MLD_T^{∇} have larger RMS differences and lower correlation. In the tropics, SLD and MLD_T^{∇} are relatively close with lower RMS differences and higher correlation. The MLD_{TS}^{Δ} is less precise (large variance) and has a deep bias relative to SLD for the entire seasonal cycle. Alternative threshold values reduce this bias.

[47] Since the MLD_T^{∇} is a curvature based methodology, deviations in the vertical gradients of temperature define the

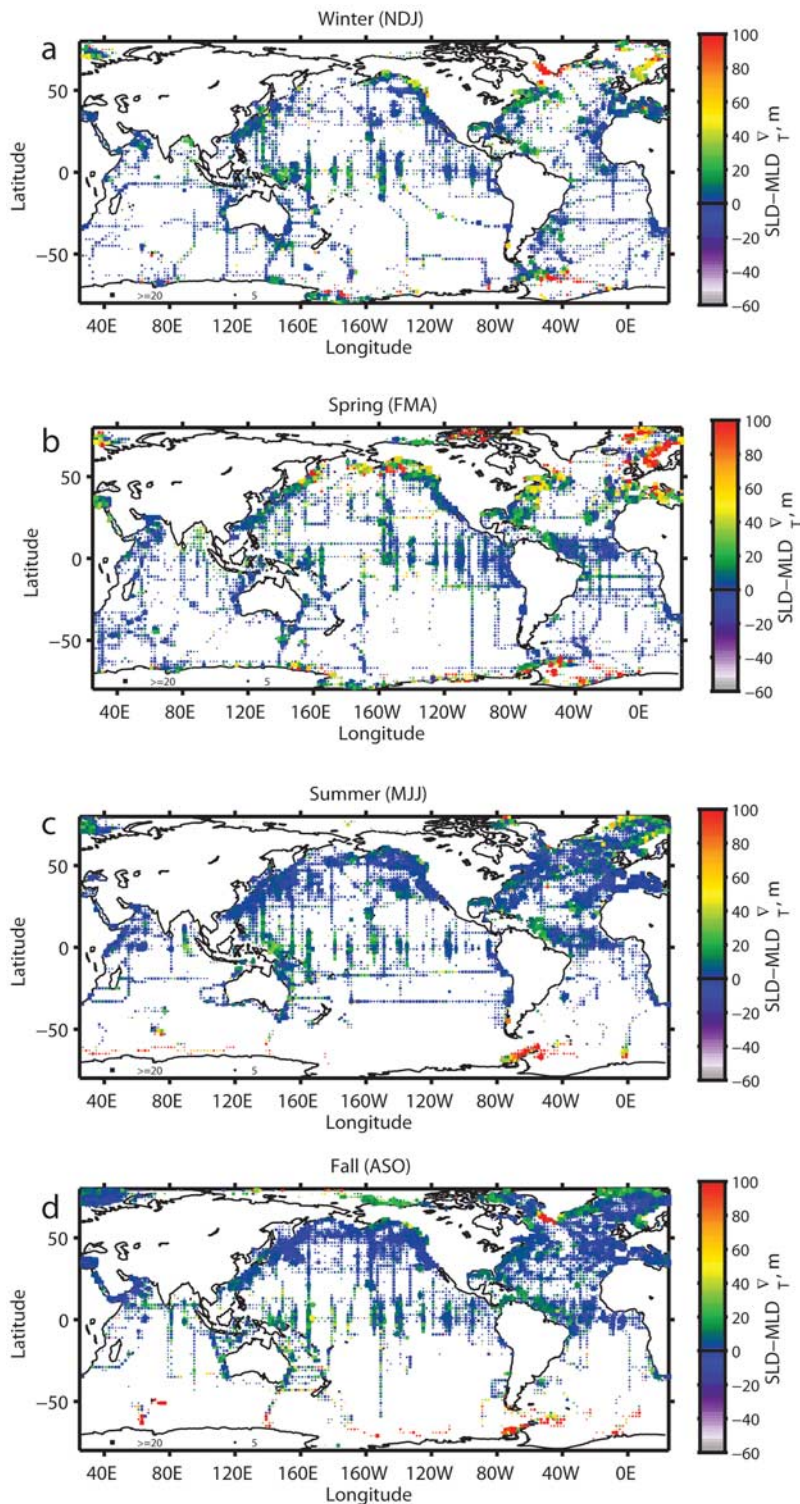


Figure 9. (a) Winter (November, December, and January), (b) spring (February, March, April), (c) summer (May, June, July), and (d) fall (August, September, and October) seasonal occurrence of $MLD_{\nabla}^{\nabla}/SLD$ differences. Each box represents a 2×2 degree region of the ocean, color coded by the average $SLD-MLD_{\nabla}^{\nabla}$ as denoted by the color bar. The size of the box represents the number of observations where the largest boxes have at least 20 observations but in some regions there are many more. The box size legend is in the lower left of each panel.

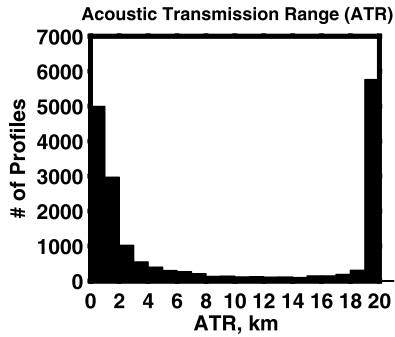


Figure 10. A histogram of 18000 ATR values (described in section 3.1) computed using the RAM for all five frequencies (section 3.2). The bin at 14 km has the fewest number of cases (94) and therefore represents the cutoff between trapping and nontrapping environments.

surface mixed layer. These sometimes small deviations, particularly during spring, can have a disproportionately large impact on MLD_T^∇ , producing a bias relative to the SLD. The threshold based MLD_{TS}^Δ does not have the

precision, evidenced by its large variance, to resolve these small vertical gradients of temperature. As a result there is a weaker seasonal cycle in the MLD_{TS}^Δ versus SLD bias.

[48] The gradient deviations identified by the MLD_T^∇ are important for characterizing the acoustics properties of the upper ocean. This is because the MLD_T^∇ made more correct predictions of acoustic trapping than the MLD_{TS}^Δ . This has many implications for the ability of numerical simulations to predict acoustic properties in addition to other practical applications that include Navy operations, acoustic communications, and tomography. In situations, where MLD is estimated only from temperature, predicting the acoustic properties of the upper ocean may be considerably uncertain, particularly in the spring and/or at high latitudes. In addition, many models have been tested against threshold base MLD algorithms [e.g., *Kara and Hurlburt, 2006*]. This analysis suggests that standard threshold MLD algorithms are often less representative of the SLD and miss some important vertical gradients of the upper ocean.

[49] Future applications of this research will entail using SLD, ATR and other RAM acoustic computations as metrics for numerical ocean predictions. The general advantage of using acoustic metrics is that they utilize the entire profile and are very sensitive to vertical gradients.

Is Trapping Observed by RAM?

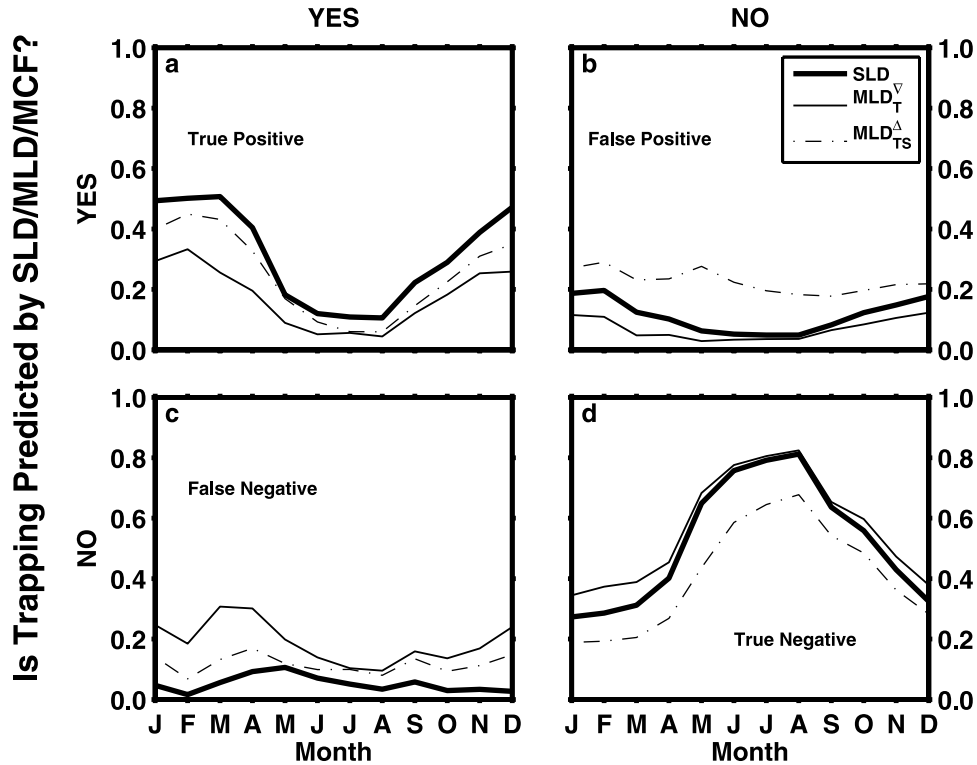


Figure 11. A 2×2 contingency table of “observed” versus “predicted” trapping from estimates of SLD, MLD, and MCF. The y axis represents the fraction of the total number of cases and the x axis represents the month. In Figure 11a True Positive indicates acoustic trapping was predicted and observed. False Positive (b) and False Negative (c) indicates trapping was predicted but not observed and not predicted but observed, respectively. True Negative (d) is where the predicted and observed both indicated no trapping. The thick line is for SLD, while the thin and the dash-dot lines are for the MLD_T^∇ and MLD_{TS}^Δ , respectively.

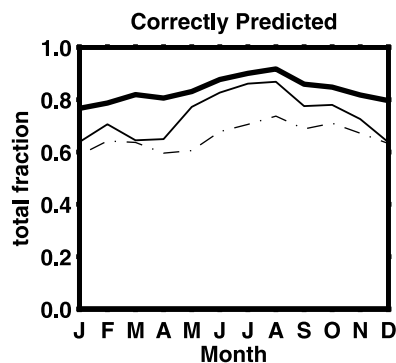


Figure 12. Total fraction of correct predictions from SLD (thick), MLD_T^{Δ} (thin), and MLD_{TS}^{Δ} (dash-dot) estimates. SLD makes the highest fraction of correct predictions.

This is value added over using a single attribute of the observed profile or ordinary RMS differences.

List of Symbols and acronyms

ATR	acoustic transmission range
c	sound speed
\bar{c}	average sound speed
CTD	conductivity temperature and depth recorder
$\Delta\sigma_t$	the threshold sigma-t value
ΔT	the threshold temperature value
f_0	minimum frequency
f_{mean}	log scale mean frequency
KRH00	Kara et al. [2000]
LDNK06	Lorbacher et al. [2006]
MCF	Minimum Cutoff Frequency
MLD	Mixed Layer Depth, in general
MLD_{TS}^{Δ}	Kara et al. [2000] Mixed Layer Depth, threshold, temperature and salinity
MLD_T^{Δ}	Lorbacher et al. [2006] Mixed Layer Depth, curvature, temperature only
RAM	Range dependent Acoustic Model
SLD	Sonic Layer Depth

[50] **Acknowledgments.** This publication is a contribution to the Improved Synthetic Ocean Profile (ISOP) project supported by the Office of Naval Research under program element 602345N. We thank the National Oceanographic Data Center and Tim Boyer for assistance with the World Ocean Database 2005 data, Ken Grembowicz of the Naval Oceanographic Office for assistance with the Master Oceanographic Observational Data Set and Jan Dastugue for help with graphics. We appreciate the careful consideration of several reviewers and their suggestions that have led to an improved manuscript. This is contribution NRL/JA/7320/2006/7048 and has been approved for public release.

References

- Bathen, K. H. (1972), On the seasonal changes in the depth of the mixed layer in the North Pacific Ocean, *J. Geophys. Res.*, *77*, 7138–7150.
- Belkin, I. M., and B. N. Filyushkin (1986), Seasonal variability of upper ocean thermal structure in the POLYMODE study Area, *Oceanology*, *26*, 149–154.
- Bovik, A. C., T. S. Huang, and D. C. Munson Jr. (1983), A generalization of median filtering using linear combinations of order statistics, *IEEE T. Acoustics Speech Signal Proc.*, *ASSP-31*, 1342–1350.

- Boyer, T. P., J. I. Antonov, H. E. Garcia, D. R. Johnson, R. A. Locarni, A. V. Mishonov, M. T. Pitcher, O. K. Baranova, and I. V. Smolyar (2006), World ocean database 2005, data report, 190 pp., NOAA Atlas NESDIS 60, U.S. Gov. Print. Off., Washington, D. C.
- Brainerd, K. E., and M. C. Gregg (1995), Surface mixed and mixing layer depths, *Deep Sea Res., Part I*, *42*, 1521–1543.
- Bucker, H. P. (1980), Wave propagation in a duct with boundary scattering (with application to a surface duct), *J. Acoust. Soc. Am.*, *68*, 1768–1772.
- Buckingham, M. J. (1991), On acoustic transmission in ocean-surface waveguides, *Philos. Trans. R. Soc. Ser. A*, *335*, 513–555.
- Collins, M. D. (1994), Generalization of the split-step Padé solution, *J. Acoust. Soc. Am.*, *96*, 382–385.
- de Boyer Montégut, C., G. Madec, A. S. Fischer, A. Lazar, and D. Iudicone (2004), Mixed layer depth over the global ocean: An examination of profile data and a profile-based climatology, *J. Geophys. Res.*, *109*, C12003, doi:10.1029/2004JC002378.
- Deser, C., M. A. Alexander, and M. S. Timlin (2003), Understanding the persistence of sea surface temperature anomalies in midlatitudes, *J. Clim.*, *16*, 57–72.
- Eden, H. F., and J. Nicol (1973), Acoustic transmission in an ocean surface duct, *J. Acoust. Soc. Am.*, *53*, 819–825.
- Etter, P. C. (2003), *Underwater Acoustic Modeling and Simulation*, 3rd ed., 424 pp., Spon Press, London.
- Garrett, C. (1996), Processes in the surface mixed layer of the ocean, *Dyn. Atmos. Oceans*, *23*, 19–34.
- Kara, A. B., and H. E. Hurlburt (2006), Daily inter-annual simulations of SST and MLD using atmospherically forced OGCMs: Model evaluation in comparison to buoy time series, *J. Mar. Syst.*, *62*, 95–119.
- Kara, A. B., P. A. Rochford, and H. E. Hurlburt (2000), An optimal definition for ocean mixed layer depth, *J. Geophys. Res.*, *105*, 16803–16821.
- Kerman, B. R. (1993), *Natural Physical Sources of Underwater Sound: Sea Surface Sound*, 750 pp., Springer, New York.
- Kerr, D. E. (1951), *Propagation of Short Radio Waves*, 728 pp., McGraw-Hill, New York.
- Lorbacher, K., D. D. Dommenges, P. P. Niiler, and A. Köhl (2006), Ocean mixed layer depth: A subsurface proxy of ocean-atmosphere variability, *J. Geophys. Res.*, *111*, C07010, doi:10.1029/2003JC002157.
- Lu, L.-G., F. Qiao, H.-X. Chen, and Y.-L. Yaun (2006), Acoustic transmission in the cold eddy in the southern East China Sea, *J. Geophys. Res.*, *111*, C11S11, doi:10.1029/2005JC003162.
- Mackenzie, K. V. (1981), Nine-term equation for sound speed in the ocean, *J. Acoust. Soc. Am.*, *70*, 807–812.
- Mao, Q., S. W. Chang, and R. L. Pfeffer (2000), Influence of large-scale initial oceanic mixed layer depth on tropical cyclones, *Mon. Weather Rev.*, *128*, 4058–4070.
- Monterey, G. I., and L. M. deWitt (2000), Seasonal variability of global mixed layer depth from WOD98 temperature and salinity profiles, data report, 56 pp., NOAA-TM-NMFS-SWFSC-296, U.S. Dep. of Commerce, National Marine Fisheries Services, Pacific Grove, CA.
- Siderius, M., M. B. Porter, P. Hurskey, V. McDonald, and the KauaiX Group (2007), Effects of ocean thermocline variability on noncoherent underwater acoustic communications, *J. Acoust. Soc. Am.*, *121*, 1895–1908.
- Siegel, D. A., S. C. Doney, and J. A. Yoder (2002), The North Atlantic spring phytoplankton bloom and Sverdrup's critical depth hypothesis, *Science*, *296*, 730–733.
- Sutton, P. J., P. F. Worcester, G. Masters, B. D. Cornuelle, and J. F. Lynch (1993), Ocean mixed layers and acoustic pulse propagation in the Greenland Sea, *J. Acoust. Soc. Am.*, *94*, 1517–1526.
- Teague, W. J., M. J. Carron, and P. J. Hogan (1990), A comparison between the generalized digital environmental model and Levitus climatologies, *J. Geophys. Res.*, *95*, 7167–7183.
- Thomson, R. E., and I. V. Fine (2003), Estimating mixed layer depth from oceanic profile data, *J. Atmos. Oceanic Technol.*, *20*, 319–329.
- Urick, R. J. (1983), *Principles of Underwater Sound*, 3rd ed., 423 pp., Peninsula, Los Altos, Calif.
- Weston, D. E., and P. B. Rowlands (1979), Guided acoustic waves in the ocean, *Rep. Prog. Phys.*, *42*, 347–387.

C. N. Barron, M. R. Carnes, R. W. Helber, and R. A. Zingarelli, Naval Research Laboratory, Stennis Space Center, Code 7323, MS 39529-5004, USA. (helber@nrlssc.navy.mil)